Kirkuk University Journal /Scientific Studies (KUJSS)
Volume 12, Issue 2, March 2017
ISSN 1992 – 0849

Study of the Possibility of Achieving the Same Per-Port Outflow in a Dividing Manifold

EMAD SEDEEQ MOHAMMED

University of Kirkuk / Faculty of Engineering / Department of Mechanical Engineering

E-mail: emads.mohammed@uokirkuk.edu.iq
emad.s.mohammeduokirkuk@gmail.com

ABSTRACT

There have been several attempts to optimise fluid flow manifolds; these, however, have shown are limited and further investigation into the efficiency of these systems is needed. This work focuses on improving the distribution manifolds efficacy in outflow division, i.e. attaining the same flow rate per each exit port of the manifold. Water has been selected to be the working fluid. A numerical investigation utilising CFD (by ANSYS Fluent R16.2) analysis into two-dimensional, incompressible, and turbulent flow has been carried out to resolve the flow manifold problem using two turbulence modelling, Standard k-ε and RNG k-ε, approaches. Four values of flow rate have been considered, which are specified by the Reynolds numbers 101×10^3, 202×10^3, 303×10^3, and 404×10^3. These values correspond to the fluid inlet velocities 0.5, 1.0, 1.5, and 2.0 m/s, respectively. The manifold configuration is defined by the given area ratio (total cross-sectional area for laterals /header cross-sectional area). Three values of area ratio are considered; these are 0.703125, 0.84375, and 0.984375. The results indicate that the flow uniformity has a reverse proportional relationship with the fluid flow rate and area ratio for all manifold arrangements. However, there is no significant effect of the flow rate increase on flow mal-distribution. Also, the use of RNG k-ε model has shown higher values of the non-uniformity coefficient than those obtained by the Standard k-ε model. The outcomes of this analysis have been compared with experimental data and a good agreement among them has been found.

Keywords: Manifold, Non-uniformity, Area Ratio, Turbulence Models, Reynolds Number.

Kirkuk University Journal /Scientific Studies (KUJSS)
Volume 12, Issue 2, March 2017
ISSN 1992 – 0849

دراسة إمكانية تحقيق تدفق متساوي خلال منافذ الخروج في مشعّب توزيع

عِمـــاد صِـدّيق مُـحمـد

جامعة كركوك / كلية الهندسة / قسم الهندسة الميكانيكية

E-mail: emads.mohammed@uokirkuk.edu.iq
emad.s.mohammeduokirkuk@gmail.com

المُـلـخّــص

هناك عدة محاولات لتحسين مشعّبات الجريان، لكنّ هذه المساعي قد ظهرت بأنّها محدودة وأنّ المزيد من التحقق في كفاءة هذه الأنظمة لا يزال مطلوباً. يركّز العمل الحالي على تحسين فعالية المشعّبات في تقسيم الجريان، أي تحقيق تدفق متساوي خلال فتحات الخروج للمشعّب. تمّ إختيار الماء ليكون مائع العمل في المشعّب. أجرِيَ إستقصاء نظري (عددي) بإستخدام ديناميك الموائع الحسابي (CFD) وبمساعدة البرنامج ANSYS Fluent R16.2، وذلك لمعالجة مسألة الجريان الإضطرابي، ثنائي البعد، واللاإنضغاطي، المتمثلة في حالة جريان المائع خلال الموزّع. تمّ إستخدام طريقتين لصياغة الإضطراب، وهما k-ε القياسي و RNG k-ε. أختُبِرَ الموزّع لأربعة معدلات تدفق للماء الداخل والمحددة بأرقام رينولدز التي هي: 101×10^3، 202×10^3، 303×10^3، 404×10^3. هذه القيم مناظرة لسرع الدخول للمائع والتي هي: 0.5 ، 1.0 ، 1.5 ، و 2.0 م/ثانية، على التوالي. إنّ شكل (ترتيب) الموزّع الحالي يُعرّف من خلال نسبة المساحة (مجموع مساحات المقطع العرضي للأنابيب الفرعية مقسوماً على مساحة المقطع العرضي للأنبوب الرئيسي). لقد أعتُبِرَت ثلاثة قيم لنسبة المساحة والتي هي: 0.703125، 0.84375، 0.984375. أظهرت النتائج علاقات تناسبية عكسية لأنتظامية (تماثلية) الجريان مع معدل تدفق الماء ونسبة المساحة. مع ذلك، فإن زيادة معدل التدفق ليس لها تأثير معتبر على سوء توزيع الجريان. كذلك، فإنّ النتائج أظهرت قيم أكبر لمعامل اللاإنتظامية في حالة استعمال نموذج الإضطراب RNG k-ε للحل من تلك القيم الناتجة بإستخدام k-ε القياسي. تمّت مقارنة النتائج الحالية مع بيانات تجريبية (سابقة) وقد وُجد توافقٌ جيد بينهم.

الكلمات المفتاحية: مشعّب، اللاإنتظامية، نسبة المساحة، نماذج إضطراب، رقم رينولدز.

Kirkuk University Journal /Scientific Studies (KUJSS)
Volume 12, Issue 2, March 2017
ISSN 1992 – 0849

Nomenclature

t	Time	second
u	Velocity component in x-direction	m/s
v	Velocity component in y-direction	m/s
p	Static pressure	N/m^2
S_m	Source term: the mass added to the continuous phase from the dispersed second phase and any user-defined sources [10].	$kg/(m^3 . s)$
g	Gravitational acceleration	m/s^2
$\overrightarrow{F}$	External body force per unit volume	N/m^3
k	Turbulence kinetic energy	m^2/s^2
G_k	Generation of turbulence kinetic energy due to the mean velocity gradients [10].	W/m^3
G_b	Generation of turbulence kinetic energy due to buoyancy [10].	W/m^3
Y_M	Contribution of the fluctuating dilatation in compressible turbulence to the overall dissipation rate [10].	W/m^3
$C_{1\varepsilon}$, $C_{2\varepsilon}$, $C_{3\varepsilon}$	Constants of the transport equation for the k-ε models	
C_μ	Constant of the turbulent and effective viscosities	
S_k	User-defined source term for the transport equation of k	W/m^3
S_ε	User-defined source term for the transport equation of ε	$W/(m^3 . s)$
Q_i	Volume flow rate for ith lateral tube	m^3/s
Q	Total volume flow rate	m^3/s
N	Number of parallel tubes (*laterals*)	
$A.R$	Area Ratio	
CFD	Computational Fluid Dynamics	
Re	Reynolds number	
D	Diameter of the manifold header	m
d	Diameter of the outlet tubes (*laterals*)	m
A	Distance from the manifold inlet to the first lateral	m
S	Distance between laterals	m
L	Manifold length (length of header)	m
H	Length of laterals	m

Greek Symbols

ρ	Fluid density	kg/m^3
$\bar{\bar{\tau}}$	Stress tensor	N/m^2
μ	Molecular viscosity	$kg/(m . s)$
μ_t	Turbulent viscosity	$kg/(m . s)$
μ_{eff}	Effective viscosity	$kg/(m . s)$
ε	Turbulence energy dissipation rate	m^2/s^3
σ_k	Turbulent Prandtl number for k	
σ_ε	Turbulent Prandtl number for ε	
α_k	Inverse effective Prandtl number for k	
α_ε	Inverse effective Prandtl number for ε	
β_i	Flow ratio for ith lateral pipe	
$\bar{\beta}$	Average flow ratio for the total parallel tubes	
Φ	Non-uniformity coefficient	

Kirkuk University Journal /Scientific Studies (KUJSS)
Volume 12, Issue 2, March 2017
ISSN 1992 – 0849

1. Introduction

Among all fluid-flow devices, manifolds are the most commonly encountered in practice, aside from valves, fittings, and pipes. Manifolds occupy major importance in numerous engineering applications including old conventional applications and modern sophisticated equipment. Even in very recent applications, the design of the participating manifolds has been treated in a casual manner. Furthermore, even when more attention has been given to manifold design, the numerical simulations have been incomplete owing to improper application of the boundary conditions. There is a clear need for an in-depth evaluation of the present status of manifold design and a determined research program to respond to the outcomes of such evaluation. A manifold is a chamber consisting of one fluid inlet and numerous fluid exits or, similarly, a chamber with many fluid inlets and a single fluid outlet. The former type may be designated as a distribution manifold while the latter is termed a collection manifold. Among all of the major design problems of fluid flow, the manifold problem still remains a primary one requiring a systematic solution method. The widespread applications involving manifolds have motivated a variety of solution methods, but these have generally been specific to the individual manifold belonging to that application. The history of solution methods that have been employed for the manifold problem is closely related to the availability and power of computational tools. Up until about 1980, one-dimensional models and corresponding algebraic solution methods were the standard. In order to enable such methods to be used as a design tool, it was necessary to make rather sweeping assumptions about the kind of the fluid flow style.

Many researchers have endeavored to attain an equal outflow distribution of fluid in dividing manifolds. Therefore, work of some of those will be reviewed. The performance investigation of flow distribution systems was performed analytically by Bajura [1] for both intake and exhaust manifolds. He employed a theoretical model for formulating dimensionless parameters describing the manifolds performance. The impacts of header configuration and Reynolds number variation on the flow allocation in a flow manifold were numerically studied by Kim et al. [2]. The manifold usage was for a liquid cooling unit utilized in an electronic pack. Three different designs of header shape were studied and the authors concluded that the triangular shape is the best one for flow division. Lu Hua [3] predicted the flow distribution in manifolds via computational modeling. He utilized many numerical methods to identify the difficulties related to the design of flow spreaders that are widely encountered in industrial

Kirkuk University Journal /Scientific Studies (KUJSS)
Volume 12, Issue 2, March 2017
ISSN 1992 – 0849

applications, e.g. the manifold used in paper manufacturing system (Fig. 1). Weitbrecht et al. [4] accomplished an analytical and empirical investigation for the water flow in a dividing and collecting manifold used for solar heating (Fig. 2). The flow was analyzed in laminar conditions and the influence of frictional pressure and energy losses on the flow allocation were the main objective of the study. A numerical emulation of flow in manifolds is also submitted by Tong et al. [5] with the aid of the CFD software CFX- 9.0. The work was achieved assuming a steady tow-dimensional and laminar flow. They focused their case studies on attaining the same flow rate division among the lateral tubes connecting the distribution and collecting manifolds. Fang et al. [6] introduced a separate model describing the physical phenomena of flow distribution in manifolds. The model was made for evaluating the pressure gradient through the manifold domain. They also conducted an empirical work to specify many parameters for the manifold performance in flow allocation at different operating conditions.

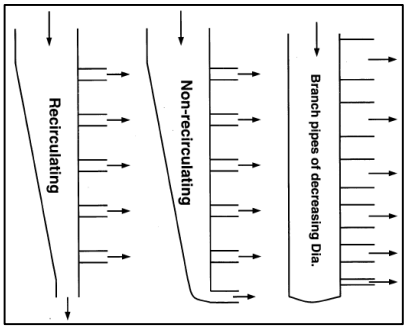

Fig. 1: Types of the manifold utilized in the head box of papermaking system.

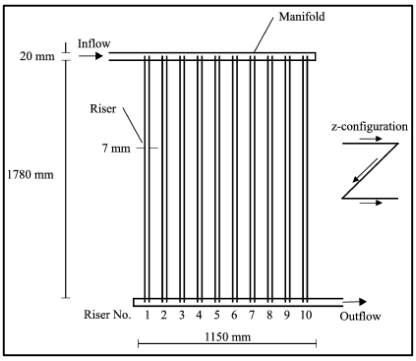

Fig. 2: Solar collector with *z*-configuration.

Andrew and Sparrow [7] studied numerically the impact of the outlet ports shape on the outflow rate equality in a dividing manifold with a circular cross-section header. The solving model selected for this aim was the realizable k-ε. They considered three geometries of the manifold exits and declared that the continual solo-slot shape is the best one for the flow uniformity. Andrew and Sparrow [8] also investigated the possibility of attainment the ideal performance of distribution manifold by two geometric methodologies. These methodologies include: (a) varying the area ratio and (b) raising the flow resistance in the lateral tubes via increasing their length-diameter ratio which eventually yields to more pressure drop (Figs. 3a & 3b). Tong et al. [9] carried out a numerical study for identifying the strategies of optimizing the manifold design to enhance its efficacy in outflow distribution. The difficulty encountered in the design was ascribed to the variations happening in fluid pressure along the header due to

Kirkuk University Journal /Scientific Studies (KUJSS)
Volume 12, Issue 2, March 2017
ISSN 1992 – 0849

the effusion of flow through the outlet tubes which results in a further decrease in fluid velocity. A generic manifold system was used as shown in the Fig. 4.

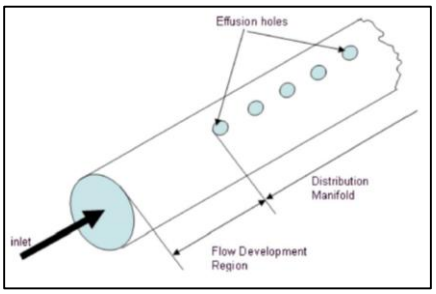

Fig. 3a: Schematic of the physical system.

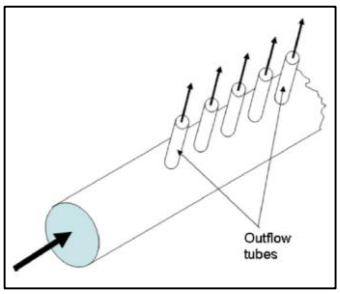

Fig. 3b: The distribution manifold fitted with outflow tubes to convey its discharge to a collection manifold.

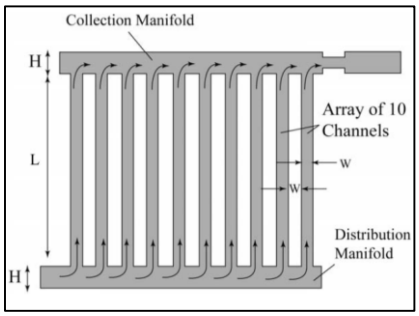

Fig. 4: A schematic diagram of a generic manifold system.

The present study has been established with the focus on the impact of area ratio and fluid flow rate on the flow distribution which differ in values from what are existent in earlier works. Also, the distinction here is in the mechanism of varying the area ratio via changing the number of laterals rather than modifying their diameter or the header dimensions. Moreover, high turbulent flow limits have been selected (extended to more than 4.0×10^5 Reynolds number) in order to test and disclose the manifold outflow uniformity in high turbulence conditions.

2. Theoretical Background

2.1. Fluid Flow Governing Equations

The physical phenomenon of fluid flow in manifolds is governed by differential equations for both continuity and momentum and they will be indicated in the next subsidiary sections.

2.1.1 The Mass Conservation or Continuity Equation

The mass conservation equation of a flowing fluid is given as indicated below [10]:

$$\frac{\partial \rho}{\partial t} + \nabla . \left(\rho \vec{V} \right) = S_m \qquad (1)$$

Equation (1) is the general equation and is applicable for incompressible and compressible flows. For special cases, i.e. problems with steady two-dimensional and incompressible flow (since the current flow problem is two-dimensional), the Eq. (1) will be reduced to a simplified form and given as follows [7],

$$\frac{\partial u}{\partial x} + \frac{\partial v}{\partial y} = 0 \qquad (2)$$

Kirkuk University Journal /Scientific Studies (KUJSS)
Volume 12, Issue 2, March 2017
ISSN 1992 – 0849

2.1.2 Momentum Conservation Equations

In an inertial or non-accelerating reference frame, the conservation of momentum is given as following [10].

$$\frac{\partial}{\partial t}\left(\rho \vec{V}\right) + \nabla.\left(\rho \vec{V}\vec{V}\right) = -\nabla p + \nabla.\left(\bar{\bar{\tau}}\right) + \rho \vec{g} + \vec{F} \quad (3)$$

For steady incompressible and turbulent flows, the equation above is formulated as the Reynolds–averaged Navier–Stokes equations (RANS) and dismantled in general into three separate equations. The present study is two-dimensional, i.e. only two components of the velocity vector are considered (just *x* and *y*). Thus, the general momentum formula (Eq. 3) is simplified to form the components of RANS equations and written in two separate equations in *x* and *y* directions as following [7]:

$$\rho\left[\frac{\partial}{\partial x}(u^2) + \frac{\partial}{\partial y}(uv) + \frac{\partial}{\partial z}(uw)\right] = -\frac{\partial p}{\partial x} + \frac{\partial}{\partial x}\left(\mu_{eff}\frac{\partial u}{\partial x}\right) + \frac{\partial}{\partial y}\left(\mu_{eff}\frac{\partial u}{\partial y}\right) + \frac{\partial}{\partial z}\left(\mu_{eff}\frac{\partial u}{\partial z}\right) \quad (4)$$

$$\rho\left[\frac{\partial}{\partial x}(vu) + \frac{\partial}{\partial y}(v^2) + \frac{\partial}{\partial z}(vw)\right] = -\frac{\partial p}{\partial y} + \frac{\partial}{\partial x}\left(\mu_{eff}\frac{\partial v}{\partial x}\right) + \frac{\partial}{\partial y}\left(\mu_{eff}\frac{\partial v}{\partial y}\right) + \frac{\partial}{\partial z}\left(\mu_{eff}\frac{\partial v}{\partial z}\right) \quad (5)$$

The effective viscosity (μ_{eff}) is defined as $\mu_{\text{eff}} = \mu + \mu_t$. Where μ_t is the eddy or turbulent viscosity, it is not a property of fluid. It differs from an application to another and relies on the chosen turbulence model. It is also considered to be isotropic in most turbulence models [7]. In the current problem two models are selected, the standard k-ε and the RNG k-ε.

2.2. Turbulence Models

2.2.1 Transport Equations for the Standard *k-ε* Model

For this model, equations used to obtain *k* and *ε* are illustrated respectively below [11]:

$$\frac{\partial}{\partial t}(\rho k) + \frac{\partial}{\partial x_i}(\rho k u_i) = \frac{\partial}{\partial x_j}\left[\left(\mu + \frac{\mu_t}{\sigma_k}\right)\frac{\partial k}{\partial x_j}\right] + G_k + G_b - \rho\varepsilon - Y_M + S_k \quad (6)$$

$$\frac{\partial}{\partial t}(\rho \varepsilon) + \frac{\partial}{\partial x_i}(\rho \varepsilon u_i) = \frac{\partial}{\partial x_j}\left[\left(\mu + \frac{\mu_t}{\sigma_\varepsilon}\right)\frac{\partial \varepsilon}{\partial x_j}\right] + C_{1\varepsilon}\frac{\varepsilon}{k}(G_k + C_{3\varepsilon}G_b) - C_{2\varepsilon}\rho\frac{\varepsilon^2}{k} + S_\varepsilon \quad (7)$$

2.2.2 Modelling the Turbulent Viscosity

The turbulent or eddy viscosity (μ_t) can be determined by incorporating *k* and *ε* together in a single formula as follows [10]:

$$\mu_t = \rho C_\mu \frac{k^2}{\varepsilon} \quad \ldots\ldots\ldots\ldots\ldots (8), \quad \textit{where } C_\mu \textit{ is a constant.}$$

Kirkuk University Journal /Scientific Studies (KUJSS)
Volume 12, Issue 2, March 2017
ISSN 1992 – 0849

2.2.3 Constants of the Standard *k-ε* Model

The constants appeared in the Eqs. (6, 7, and 8) have established default values given by Fluent [10]: $C_{1\varepsilon}$ = 1.44, $C_{2\varepsilon}$ = 1.92, C_{μ} = 0.09 σ_k = 1.0, and σ_{ε} = 1.3.

2.2.4 Transport Equations for the RNG *k-ε* Model

Equations concerning the determination of k and ε are constructed respectively for the RNG model as follows [12, 13]:

$$\frac{\partial}{\partial t}(\rho k) + \frac{\partial}{\partial x_i}(\rho k u_i) = \frac{\partial}{\partial x_j}\left(\alpha_k \mu_{eff} \frac{\partial k}{\partial x_j}\right) + G_k + G_b - \rho\varepsilon - Y_M + S_k \quad (9)$$

$$\frac{\partial}{\partial t}(\rho \varepsilon) + \frac{\partial}{\partial x_i}(\rho \varepsilon u_i) = \frac{\partial}{\partial x_j}\left(\alpha_\varepsilon \mu_{eff} \frac{\partial \varepsilon}{\partial x_j}\right) + C_{1\varepsilon}\frac{\varepsilon}{k}(G_k + C_{3\varepsilon}G_b) - C_{2\varepsilon}^{*}\rho\frac{\varepsilon^2}{k} \quad (10)$$

$$Where,\ C_{2\varepsilon}^{*} = C_{2\varepsilon} + \frac{C_\mu \eta^3 (1-\eta/\eta_0)}{1+\beta\eta^3}\ ,\quad and,\ \eta = \frac{S_k}{\varepsilon}\ ,\ \eta_0 = 4.38\ ,\beta = 0.012 \quad (11)$$

For the high-Reynolds-number limit, both α_k *and* α_ε are taken nearly as 1.393 [10].

2.2.5 Modelling the Effective Viscosity

In the high-Reynolds-number limits, the values of the effective viscosity and the turbulent viscosity become approximately identical. Thus, the effective viscosity can be found from the Eq. (8) with C_μ = 0.0845. The C_μ value is derived using RNG theory [10].

2.2.6 RNG *k-ε* Model Constants

The constants $C_{1\varepsilon}$, $C_{2\varepsilon}$ in the Eqs. (10, 11) have the following default values used by Fluent; $C_{1\varepsilon}$ = 1.42, $C_{2\varepsilon}$ = 1.68. These values are derived analytically via the RNG theory [10].

2.3. Non-Uniformity Flow Coefficient (Φ)

The manifold efficacy in flow distribution is evaluated by means of the dimensionless factors, Φ and βi. They are defined as follows [14]:

$$\varphi = \sqrt{\frac{\sum_{i=1}^{n}(\beta_i - \bar{\beta})^2}{N}} \qquad where,\ \ \beta_i = \frac{Q_i}{Q}\ \ ;\ \ and,\ \ \bar{\beta} = \frac{\sum_{i=0}^{n}\beta_i}{N} \quad (12)$$

The large value of Φ implies more flow mal-distribution, and thus the minimum value of non-uniformity coefficient gives the optimum design configuration for the manifold.

The header-tube area ratio (A.R) has been defined as the ratio of the total cross-sectional area for all exit ports to the header cross-sectional area, it can be determined as follows [14]:

$$A.R = N \times \left(\frac{d}{D}\right)^2 \quad (13)$$

Kirkuk University Journal /Scientific Studies (KUJSS)
Volume 12, Issue 2, March 2017
ISSN 1992 – 0849

3. Grid Creation and Validation

The grid was generated for each manifold arrangement case using quadrilateral cells. An inflation was made for flow domains near wall boundaries to enhance the mesh quality and get solutions in the boundary layer regions. The bias factor of the layers inflation has been selected to be equal 40 for the horizontal walls and 20 for the vertical walls. The mesh generation is indicated in Fig. 5. The mesh quality was validated via knowing some of the main quality measures like warping factor, skewness, and orthogonal quality of the elements (cells) for each case of the manifold arrangement. Table 1 shows grid statistics for all manifold configurations.

4. The CFD Model and Simulation Approach

The manifold with the configuration indicated by the Fig. 6 has been prepared. Thereafter, the simulation was done by the CFD based software ANSYS Fluent R16.2– ACADEMIC to process the flow problem. Firstly, the geometry of the manifold was sketched, and then the mesh sizing was performed to produce 161255 elements as the maximum size for the overall flow domain. The program setup has been carried out with the following specifications:

- **Assumptions:** Steady two-dimensional fluid flow, Incompressible flow, Fully developed flow at the manifold entrance, Gravitational effects due to fluid mass and the effects of molecular viscosity are negligible.
- **CFD Simulation:** 2ddp (two-dimensional double precision), Serial Processing.
- **Solver:** Pressure-based, Absolute Velocity Formulation, Steady Flow, Planar 2D Space.
- **Solution Turbulence Models:** Standard *k-epsilon*, and RNG *k-epsilon* Models, EWT.
- **Working Fluid (Materials):** Water-liquid, Temperature =18 ^{o}C, Density=998.2 kg/m^3, Viscosity = 0.001003 kg/ (m. s).
- **Solution Method:**

- Pressure-Velocity Coupling: SIMPLE Scheme.
- Spatial Discretization: Least Squares Cell-Based Gradient, Pressure ≡ Second Order, Momentum Equation Setting ≡ Second Order Upwind, Turbulent Kinetic Energy (k) ≡ Second Order Upwind, Turbulent Dissipation Rate (ε) ≡ Second Order Upwind.

- **Convergence Absolute Criteria:**

- Continuity = 1E -06 , X– Velocity = 1E -06
- Y– Velocity = 1E -06 , k = 1E -06 , epsilon (ε) = 1E -06

Kirkuk University Journal /Scientific Studies (KUJSS)
Volume 12, Issue 2, March 2017
ISSN 1992 – 0849

Table 1: Mesh statistics and metric for the problem domain.

Manifold Arrangement	Total Elements	Total Nodes	Cells Shape Type	Warping Factor	Skewness	Orthognal Quality
Case 1 A.R = 0.703125	115480	119193	Quadrilateral	Min = Zero Max = Zero Average = Zero Standard Deviation =Zero	Min = 1.3586e-010 Max = 0.97231 Average = 0.06884 Standard Deviation = 0.10863	Min = 0.17714 Max = 1.0 Average = 0.98345 Standard Deviation = 0.062874
Case 2 A.R = 0.84375	137094	141544	Quadrilateral	Min = Zero Max = Zero Average = Zero Standard Deviation =Zero	Min = 6.9572e-005 Max = 0.94595 Average = 0.066662 Standard Deviation = 0.10957	Min = 0.18279 Max = 1.0 Average = 0.98375 Standard Deviation = 0.06342
Case 3 A.R = 0.984375	161255	166391	Quadrilateral	Min = Zero Max = Zero Average = Zero Standard Deviation =Zero	Min = 1.4012e-005 Max = 0.97311 Average = 0.064013 Standard Deviation = 0.10763	Min = 0.18274 Max = 1.0 Average = 0.98432 Standard Deviation = 0.061826

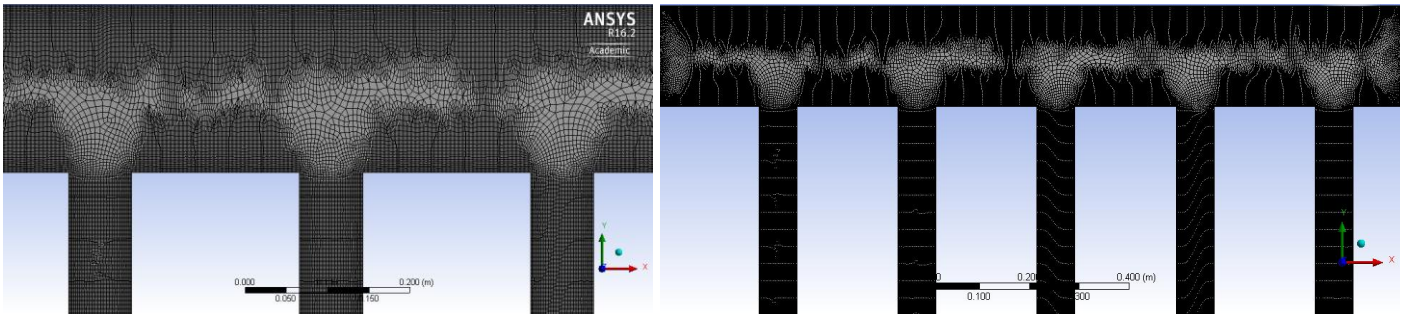

Fig. 5: The mesh generation for the first manifold configuration, A.R = 0.703125.

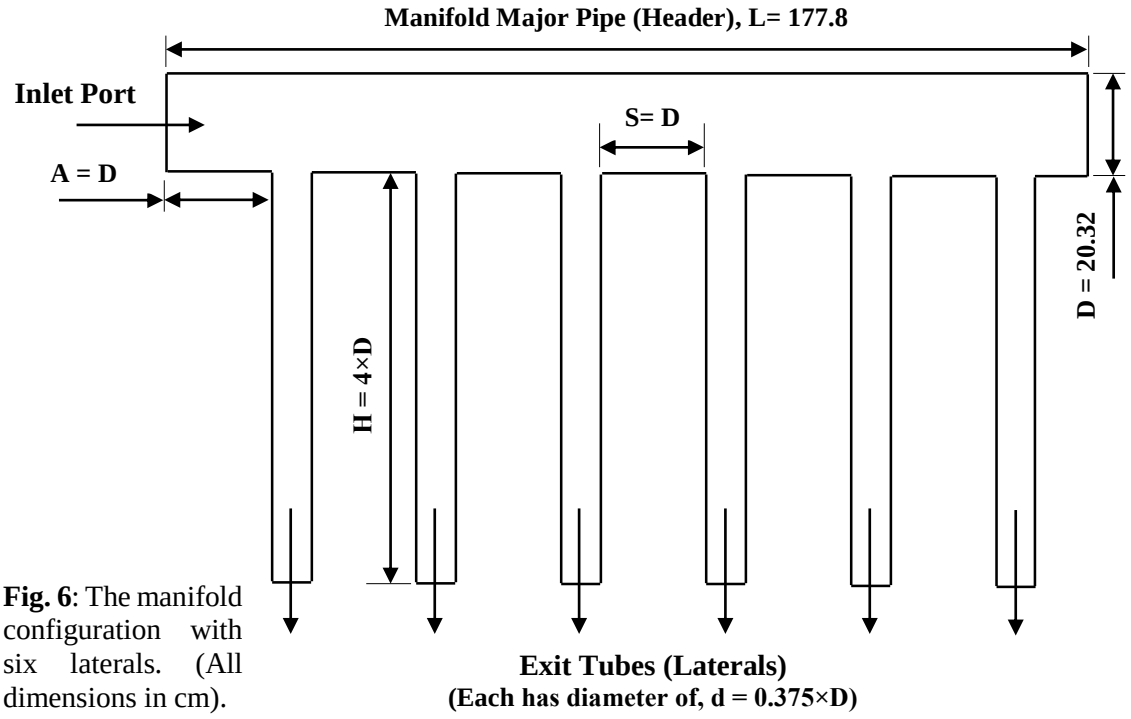

Fig. 6: The manifold configuration with six laterals. (All dimensions in cm).

Kirkuk University Journal /Scientific Studies (KUJSS)
Volume 12, Issue 2, March 2017
ISSN 1992 – 0849

4.1 Problem Boundary Conditions

The boundary conditions considered in the simulating program are summarized in Table 2.

Table 2: The boundary conditions for the manifold with all design configurations.

Boundary Condition	Test 1	Test 2	Test 3	Test 4
Reynolds Number	101113.7787	202227.5574	303341.3360	404455.1147
Entry Volume Flow Rate (L / s)	16.21463934	32.429278663	48.6439180	64.85855733
Inlet Water Temperature (°C)	18	18	18	18
Fluid Outlet Gauge Pressure	Zero	Zero	Zero	Zero

5. Results and Discussion

5.1. Effect of the Outlet Tube Number on the Flow Ratio

The flow ratio is a measure of the fluid flow uniformity and indicates how much fluid each lateral tube can receive. In Figs. 7, 8, and 9, the relation between outlet tube number and the fluid flow ratio is represented. As illustrated by them, a clear positive relationship is found for all values of flow rates and for both standard and RNG k-ε models. The flow ratio indicates low values for the first outlet tube and increases dramatically by the second and third one and this rise decreases gradually after the third lateral for all existent designated area ratios. This is imputed to the flow pattern at the header inlet. When the fluid enters the header with high velocity (high turbulent flow), this results in forming a solo jet flow. The static pressure decreases as a result of the high fluid momentum at the upper stream and hence the variance in pressure between the inlet and outlet ports will diminish. This what interprets the low values of flow ratio for the laterals nearest to the manifold inlet. Also, by comparing the three figures we can prove that for the same outlet number the flow ratio is different especially in first three laterals, this is due to impact of the difference in the area ratio for each manifold configuration. For instance, with A.R= 0.703 and for outlet number =2, β takes almost 0.06 while it is near 0.036 and 0.015 when A.R is 0.844 and 0.9844, respectively. The previous clarifications are valid for all values of flow rates and with both turbulence models. A remarkable noticing can be found from the prior discussed figures, that is, for a specific value of outlet number and area ratio the values of β are almost identical with all Reynolds numbers and for both the turbulence solution models, this what makes us able to decide that the variations in flow rate have no considerable effect on the flow ratio.

Kirkuk University Journal /Scientific Studies (KUJSS)
Volume 12, Issue 2, March 2017
ISSN 1992 – 0849

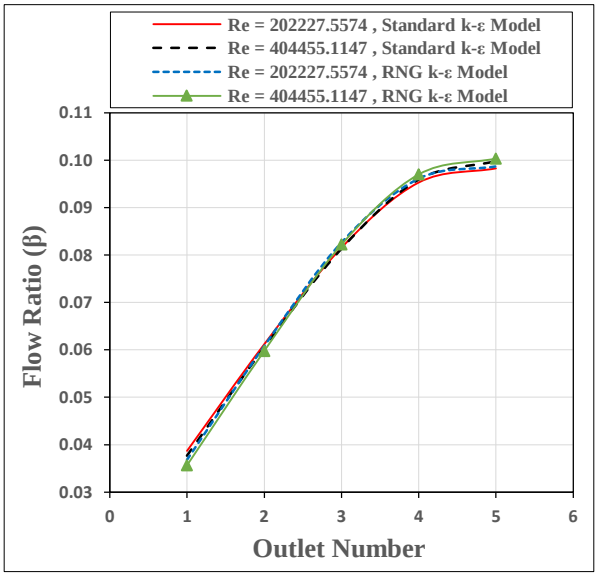

Fig. 7: Outlet tube number versus fluid flow ratio for various inlet flow rates. A.R = 0.703125.

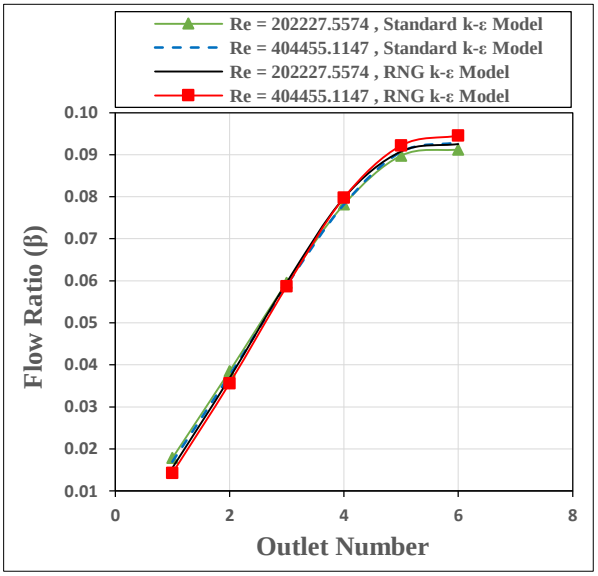

Fig. 8: Outlet tube number versus fluid flow ratio for various inlet flow rates. A.R = 0.84375.

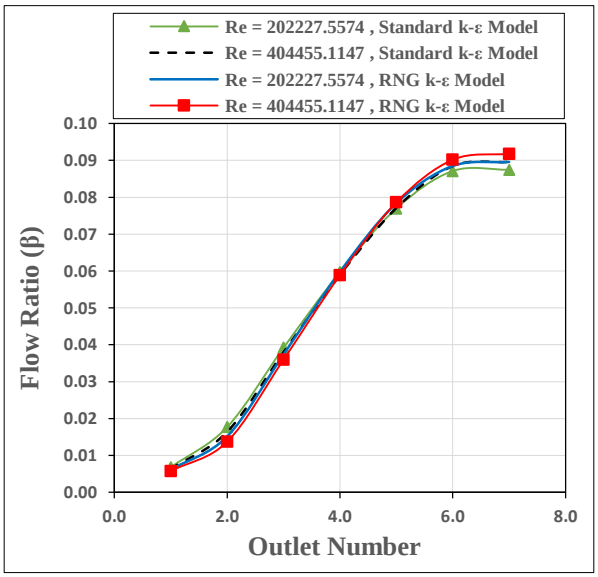

Fig. 9: Outlet tube number versus fluid flow ratio for various inlet flow rates. A.R = 0.984375.

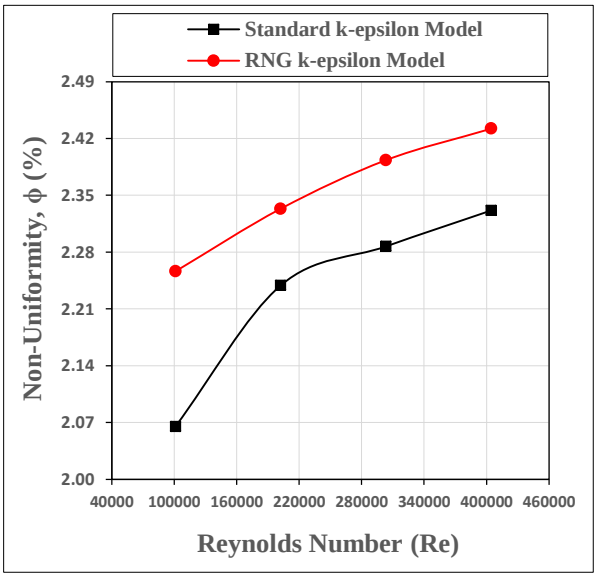

Fig. 10: Effect of water flow rate at the manifold inlet on the flow uniformity for A.R = 0.703125.

Another essential observation the findings comprise, for the latest three laterals, the β values are nearly same regardless of the area ratio and the curves exhibit different behavior in comparison with their pattern in other regions, their slope is degraded gradually and for the two last tubes the curves show approximately linear behavior and hence the β values remain constant at about 0.10 for the first manifold configuration and near 0.09 for the remaining configurations. This contrast in the curves patterns can be interpreted by the large amount of the momentum

Kirkuk University Journal /Scientific Studies (KUJSS)
Volume 12, Issue 2, March 2017
ISSN 1992 – 0849

the fluid carries at the wall of the closed end of the header which forces the fluid to enter the lateral with more mass. Moreover, the resistance occurred by the wall makes the fluid to reverse its flow direction which results in more flow rate and more flow equality at the last two exit ports, this what explicates the more uniform flow pattern at the latest two laterals.

5.2. Effect of the Fluid Inlet Flow Rate on the Outflow Uniformity

Figures 10, 11, and 12 indicate the effect of the fluid flow rate at the manifold inlet on the non-uniformity coefficient for both preceding mentioned turbulence models and various area ratios. It is obvious from the graphs that the non-uniformity is affected by the flow rate variations which is clarified by the values of Reynolds number, and as the flow rate increases the non-uniformity increases too, this is due to small time period allowed to the fluid to spread uniformly through the outlet tubes (laterals) and because of the increased fluid momentum by the Reynolds number raise (higher turbulence), this results in push the fluid particles away from the first and second outlet tubes and hence causing further non-uniformity. The figures of Φ are higher for the RNG *k*-*ε* turbulence model than those of the standard *k*-*ε*, this is attributed to the refinements included within the RNG model regarding the effect of swirl on turbulence and the effective viscosity that accounts for effects of low-velocity regions. Furthermore, an additional term included in *ε* equation of the RNG model which has a significant effect on the accuracy of model solution which considers an extra influence for rapidly strained flows.

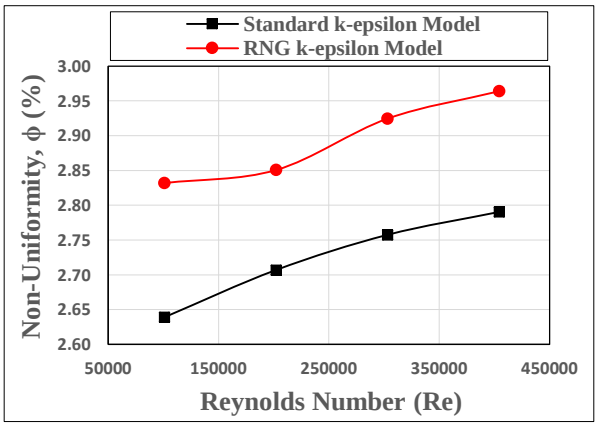

Fig. 11: Effect of water flow rate at the manifold inlet on the flow uniformity for A.R = 0.84375.

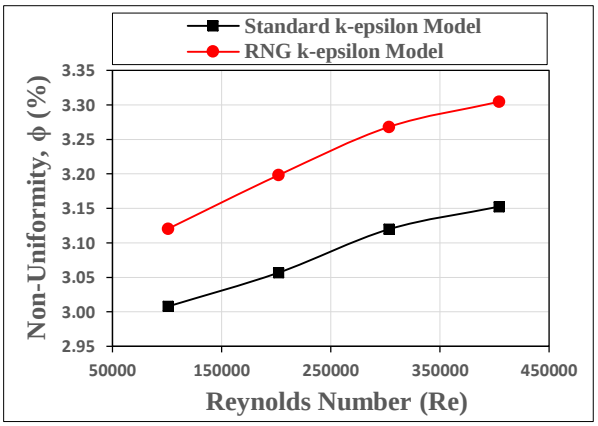

Fig. 12: Effect of water flow rate at the manifold inlet on the flow uniformity for A.R = 0.984375.

For Re = 10^5, the value of non-uniformity is near 0.02 for the standard *k*-*ε* model while it is 0.0225 with the RNG *k*-*ε*, this is for A.R=0.703125. The figures of Φ become larger with higher values of Reynolds number for all amounts of area ratio. It is clear from the previously

mentioned Figures (i.e. 10, 11, and 12) that the curves of Φ-Re have more linearity for the RNG *k-ε* model than the curves obtained by the standard *k-ε*. This is an advantage recorded for the first one, where the linearity feature is an important property for any graph which makes the extrapolation of figures more easily. Therefore, we can conclude that the RNG turbulence model is the best one for evaluating the flow problem presented here although it gives worse results for the flow uniformity.

Another substantial observation can be found, that is when the fluid accelerates so that the Reynolds number becomes in the range of 3×10^5 to 4×10^5 (i.e. for high Reynolds numbers), the increase of Φ becomes slight in comparison with its value for the Re increase range of 1×10^5 to 2×10^5. The explanation for this trend of the flow uniformity is related to the high viscous friction associated with the high turbulent flow which results in more increase of flow resistance in the laterals and hence the best chance for uniform flow distribution. This comparison is almost valid with all existing area ratios.

5.3. Effect of the Area Ratio on the Fluid Outflow Uniformity

The area ratio has a significant role in evaluating the uniformity of fluid flowing through manifolds. It gives a good measure for designing configurations as well as the fluid flow patterns. The relation curves of the non-uniformity coefficient versus the area ratio for various inlet flow rates are given in the Figs. 13 and 14. It is evident from the graphs that the values of Φ rise as A.R values progress for all Re curves and with both relied solution models. This increase in Φ can be interpreted as follows: as the area ratio increases with the same flow rate value, the chance of fluid to distribute uniformly reduces due to further decrease in static pressure as clarified by contour plots (Fig. 17), this diminution in static pressure is associated with an increase in dynamic pressure that responsible on fluid diffusion through the conduits (parallel tubes). Also, the increase in A.R by outlet's number increase will cause extra losses in fluid energy due to the plenty of edges included with laterals inlet and also it leads to further sudden expansion and contraction problems of the fluid. However, this brief explanation may be not sufficient to clarify the Φ–A.R effect relation because of huge considerations may be existent within the flow problem concerning eddies and different forces acting on fluid particles that govern their flow patterns.

Kirkuk University Journal /Scientific Studies (KUJSS)
Volume 12, Issue 2, March 2017
ISSN 1992 – 0849

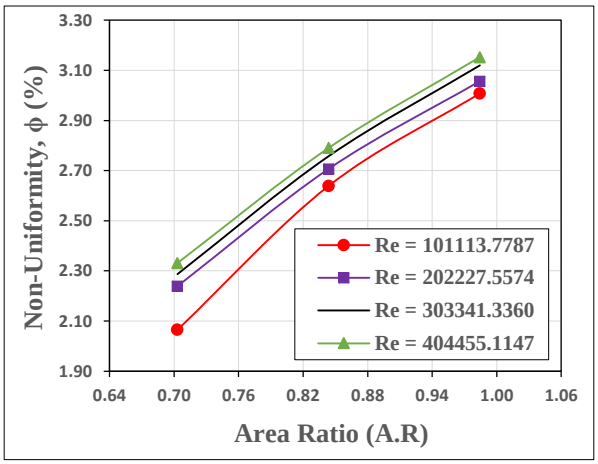

Fig. 13: The non-uniformity coefficient versus area ratio for different inlet flow rates. The Solution Model is the Standard k-ε.

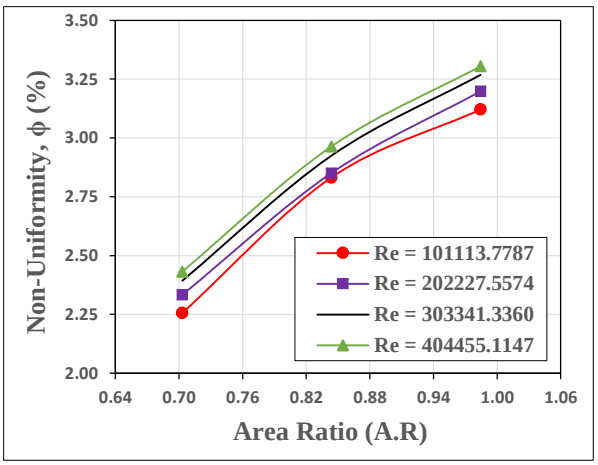

Fig. 14: The non-uniformity coefficient versus area ratio for different inlet flow rates. The Solution Model is the RNG k-ε.

For values of A.R near 0.7 with Re ≈ 4×10^5, Φ takes almost 2.3%, and with increasing A.R to 0.8 with the same Re the figures of Φ become nearly 2.6%, and when a further increase of A.R to about 1.0 the non-uniformity progresses to reach nearly 3.3%. An important conclusion the figures comprise, that is, the slope of curves decreases slowly after A.R reaches 0.82 which results in a small increment in Φ. This what is confirmed by Φ values in Fig. 14. e.g. for Re ≈ 4×10^5 and the A.R range of 0.7 to 0.82 the change in Φ values is nearly 0.5%; while this change of the non-uniformity equals 0.4% for the A.R range of 0.83 to 0.985. The recent observation is considered as a good feature and an appropriate inference to judge that a further increase in A.R could give the smallest increment in Φ by an extrapolation of the curve and hence the maximum misdistribution of flow at a certain value of A.R may be defined.

5.4. Present Findings versus Antecedent Works

Among many studies concerning the flow uniformity in manifolds, presentations of fluid distributers with the current manifold dimensions and flow ranges have not been found so far, therefore, comparisons are introduced with studies closer to the present work which were presented by Wang et al. [14, 15]. Their manuscripts include the study of flow uniformity in a distribution manifold used in compact parallel flow heat exchangers. A rectangular cross section shape header with nine parallel tubes was used to construct the manifold with water as working fluid. The investigation has been done experimentally and numerically and the effect of area ratio and the fluid flow rate was included. Low turbulent flow limits were examined

(Reynolds number ranges = 2640 up to nearly 11000) due to the small dimensions associated with the manifold. The comparison is achieved according to the dimensional and geometric similarity. The important ratio (area ratio) is approximately identical for the current manifold and that presented by the aforesaid researchers [15], and for average entry velocity of 0.83 m/s the two works can be compared. Fig. 15 indicates the variation of flow ratio with the laterals for fluid entry mean velocity of 0.83 m/s and nearly 0.80 area ratio for the two manifolds, the RNG solution model is considered for the current study.

It is clear from Fig. 15 that the values of flow ratio given by Wang et al. [15] are greater than those of the present study and the curve is less inclined especially when the fluid reaches the third tube, this is due to the small size of the selected manifold which increases the viscous flow resistance and static pressure drop at the laterals and hence more uniform distribution of the fluid through the laterals will occur. Also, the low turbulent limits taken have a substantial role in flow allocation, where at low turbulent flow the higher opportunity of uniform flow division will exist. However, a good conforming is found between the mentioned experimental work and the current numerical results particularly in the behavior of flow ratio curve. The two works exhibit roughly the same curve trend and the difference only in the values of flow ratio which is attributed to assumptions considered in the numerical study for solution facilitation that are not encountered in the empirical investigation.

Fig. 16 illustrates results of the two mentioned compared works regarding the non-uniformity coefficient. The curves indicate a contrast in Φ values and nearly the same behavior. For instance, when the entry mean velocity is 0.20 m/s, the non-uniformity coefficient records 0.025 and 0.0207 for the current work and that presented by Wang et al. [15] respectively; while at a velocity of 0.83 m/s the Φ values are 0.02847 and 0.0332, respectively. This difference is ascribed to the nearly laminar flow at 0.20 m/s inlet velocity for the manifold examined by Wang et al. [15], thus the more uniform distribution of the fluid can occur and lower values of Φ result. But for the present manifold, the flow is more turbulent at the same 0.20 m/s inlet velocity (nearly 40400 Reynolds number) and hence Φ values will be larger. After the fluid velocity reaches 0.3 m/s, the experimental results of Φ have higher values than those obtained by the numerical procedure (current work), this is due to the aforementioned reason which is expounded by few assumptions that are made to get the numerical solution. Anyway, the two results have a good congruence as long as the curves have roughly the same trend.

Kirkuk University Journal /Scientific Studies (KUJSS)
Volume 12, Issue 2, March 2017
ISSN 1992 – 0849

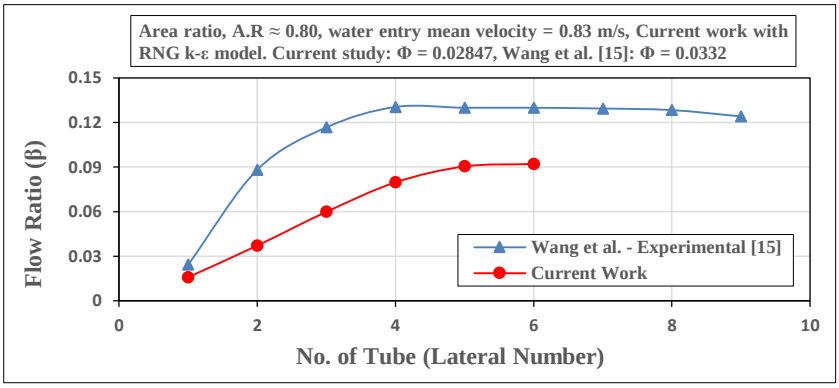

Fig. 15: Flow ratio versus outlet number. Present results and Wang et al. [15] results.

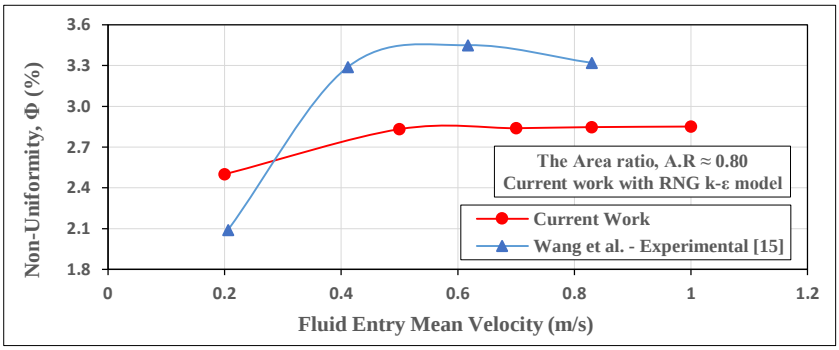

Fig. 16: Non-uniformity coefficient versus water average inlet velocity. Present results and Wang et al. [15] experimental results.

6. Conclusions

The objective of this work is to attain equal outflow rate per each exit port of the manifold. Therefore, the impact of the change of some hydraulic and geometric parameters has been tested to show their effects on the flow misdistribution through the manifold. From the previous discussions to the results in section five, we can deduce that the uniformity of fluid per-port outflow is affected by the inlet flow rate and it indicates a reverse relation, but the variations in fluid flow rate do not lead to a significant increase in the non-uniformity flow coefficient. This is almost observed with both turbulence models and for all existent area ratios. The study also indicates that the values of non-uniformity coefficient are higher with RNG k-ε model than those obtained utilizing the standard k-ε. This is valid with all manifold configurations and all selected flow rates. The area ratio (which identifies the manifold arrangement) has a serious influence on the fluid outflow uniformity, and its increase lowers the probability of obtaining the same per-port outflow. Nevertheless, the increase of area ratio through rising the laterals number may lead to identifying the largest outflow mal-distribution.

Kirkuk University Journal /Scientific Studies (KUJSS)
Volume 12, Issue 2, March 2017
ISSN 1992 – 0849

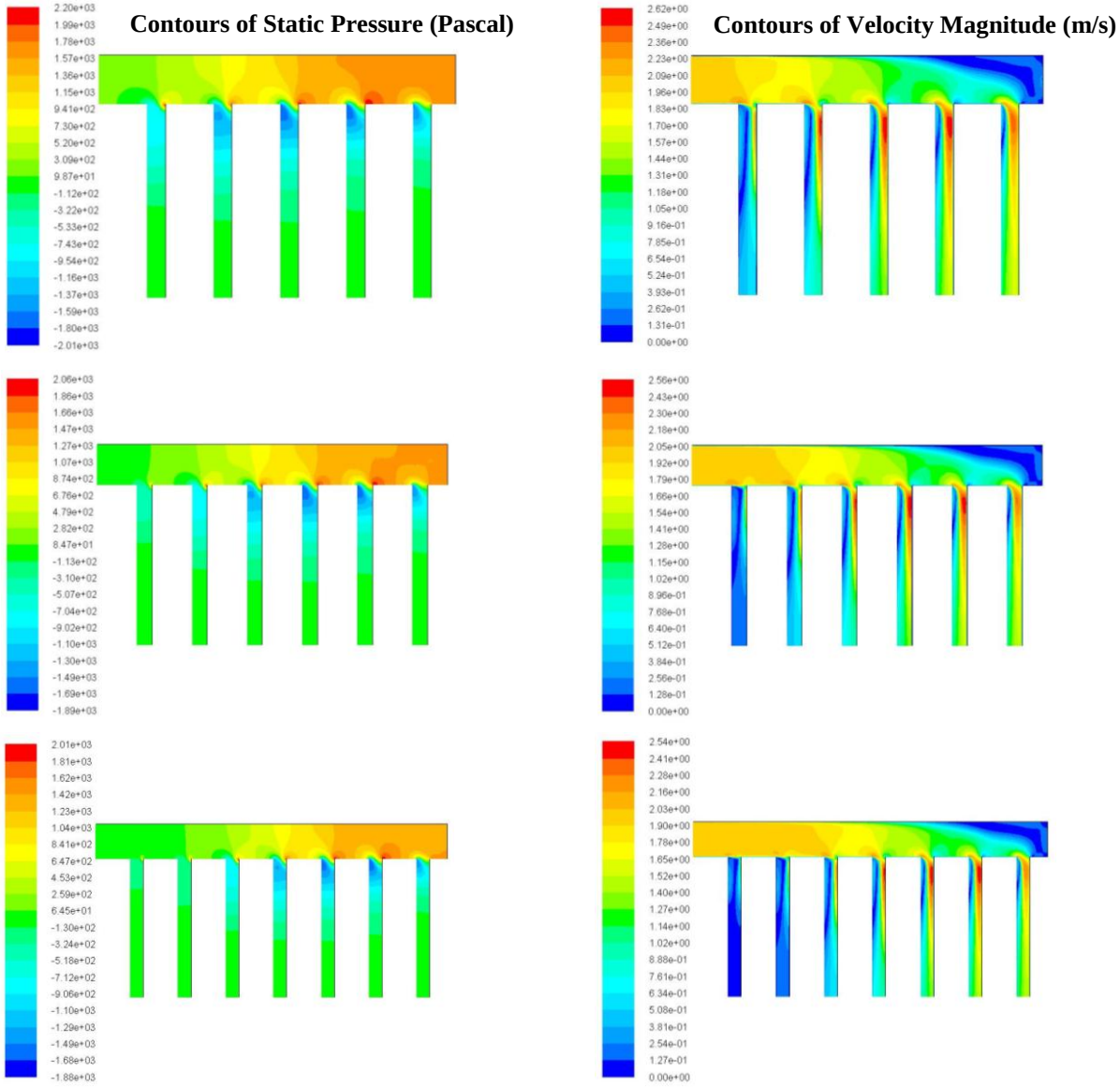

Fig. 17: Contours of Static Pressure and Velocity Magnitude for the fluid (water) in the Manifold. (RNG k-ε Model, Re = 404455.1147 & A.R = 0.703125, 0.84375, and 0.984375 respectively).

References

[1] R. A. Bajura. A model for flow distribution in manifolds. Journal of Engineering for Power, 1971; 93(1): 7–12.

[2] S. Kim, E. Choi, Y. I. Cho. The effect of header shapes on the flow distribution in a manifold for electronic packaging applications. International Communications in Heat and Mass Transfer, 1995; 22(3): 329–341.

[3] Lu Hua. Computational Modeling of Manifold Type Flow-spreaders. MSc Thesis, the University of Columbia, 1998.

[4] V. Weitbrecht, D. Lehmann, A. Richter. Flow Distribution in Solar Collectors with Laminar Flow Conditions. Solar Energy, 2002; 73(6): 433–441.

[5] Jimmy C.K. Tong, Ephraim M. Sparrow, John P. Abraham. Attainment of Flow rate Uniformity in the Channels That Link a Distribution Manifold to a Collection Manifold. Transactions of the ASME, Journals of Fluids Engineering, 2007; 129(9): 1186–1192.

[6] L. Fang, L. Yong-hao, Y. Shi-ming. Analytical and Experimental Investigation of Flow Distribution in Manifolds for Heat Exchangers. Journal of Hydrodynamics, 2008; 20(2): 179–185.

[7] Andrew W. Chen, Ephraim M. Sparrow. Effect of Exit-port Geometry on the Performance of a Flow Distribution Manifold. Applied Thermal Engineering, 2009; 29(13): 2689–2692.

[8] Andrew W. Chen, Ephraim M. Sparrow. Systematic Approaches for Design of Distribution Manifolds Having the Same Per-Port Outflow. Transactions of the ASME, Journals of Fluids Engineering, 2009; 131(6): 061101–061101–9.

[9] Jimmy C.K. Tong, Ephraim M. Sparrow, John P. Abraham. Geometric Strategies for Attainment of Identical Outflows Through All of The Exit Ports of a Distribution Manifold in a Manifold System. Applied Thermal Engineering, 2009; 29(17–18): 3552–3560.

[10] ANSYS Fluent Theory Guide – Release 16.2, ANSYS Inc., Southpointe, 2600 ANSYS Drive, Canonsburg, PA 15317, July 2015.

[11] B. E. Launder, D. B. Spalding. Lectures in Mathematical Models of Turbulence. Academic Press، London, England, 1972.

[12] S. A. Orszag, V. Yakhot, W. S. Flannery, F. Boysan, D. Choudhury, J. Maruzewski, B. Patel. Renormalization Group Modeling and Turbulence Simulations. In International Conference on Near–Wall Turbulent Flows. Tempe, Arizona, 1993.

[13] V. Yakhot, Steven A. Orszag. Renormalization group analysis of turbulence. I. Basic theory. Journal of Scientific Computing, 1986; 1(1): 3–51.

[14] C.-C. Wang, K.-S. Yang, J.-S. Tsai, I. Y. Chen. Characteristics of flow distribution in compact parallel flow heat exchangers, part I: Typical inlet header. Applied Thermal Engineering, 2011; 31(16): 3226–3234.

[15] C.-C. Wang, K.-S. Yang, J.-S. Tsai, I. Y. Chen. Characteristics of flow distribution in compact parallel flow heat exchangers, part II: Modified inlet header. Applied Thermal Engineering, 2011; 31(16): 3235–3242.